Elongational viscosity at a constant elongational strain rate of polypropylene melt

Osamu Ishizuka and Kiyohito Koyama
Faculty of Engineering, Yamagata University, 4-3-16 Jyonan, Yonezawa, 992, Japan
(Received 20 February 1979; revised 27 March 1979)

The measurement of elongational viscosity has been carried out with an improved elongational rheometer, sensitive to small elongational forces and measuring simultaneously the diameter of elongating samples. Force distribution was evaluated for various conditions. The method of reduced variables, successful in linear viscoelastic properties, can be applied to the temperature dependence of elongational viscosity only at small elongational strain rate. For large elongational strain rates, the elongational viscosity was found to be non-linear and a new method characterizing non-linearity was proposed. The non-linearity parameter in elongational viscosity was independent of elongational strain rate and almost independent of temperature. Non-linearity in elongational viscosity is discussed in terms of a structural change in the polymer melt.

INTRODUCTION

The elongation of polymer melts is important in industrial processes which include melt spinning or film blowing, and is of scientific interest. The concept of elongational viscosity was first introduced by Trouton[1] in 1906 in a study of pitch, tar and similar substances descending under their own weight. Later, Ballman[2] carried out elongational tests for rubbery polystyrene and found a constant elongational viscosity. For polymer melts, elongational experiments present complex problems: the difficulty of clamping the melt without necking; large gravitational effects on tension; and the question of conducting large strain and constant strain rate experiments. These problems were solved by Meissner[3,4]: elongational viscosity was measured for low density polyethylene containing long branches. The specimen was a rod of molten polymer floating on a silicon oil bath and was held by two pairs of gears. The portion of the specimen remaining between the gears was stretched at a constant elongational strain rate by a pair of gears rotating at a constant angular velocity. Meissner reported that elongational viscosity–time curves were S-shaped. Elongational viscosity data for various elongational strain rates were superposed at the beginning of elongational viscosity growth and almost coincided with the linear viscoelastic curve, i.e. the curve shows elongational viscosity to be three times the shear viscosity at very low shear strain rate. After considerable time, however, elongational viscosity rose quite markedly from the superposed curve and ultimately the specimen broke. Recently, similar elongational viscosity behaviour has been reported for other polymers by Everage and Ballman[5] and by Ide and White[6], who used a simplified apparatus. Everage and Ballman[5] observed that the onset of rapid elongational viscosity growth occurred at the critical value of total strain ($\gamma_c = 0.9$) which was independent of elongational strain rate. The total strain at which viscosity became 10% greater than the linear viscoelastic curve was defined as the critical elongational strain. However, the exact definition of γ_c is somewhat difficult here because elongational viscosity in the vicinity of the γ_c point deviates asymptotically from the linear superposed curve. Ide and White[6] discussed in particular the fracture behaviour of polymer melts.

In this study, the elongational viscosity of polypropylene was measured at various temperatures and elongational strain rates, using an improved apparatus which was designed to obtain more accurate elongational viscosities. Constant elongational strain rates were confirmed by the simultaneous measurement of sample diameter. A new definition of critical elongational strain is presented and the temperature and the elongational strain rate dependent on γ_c are discussed.

EXPERIMENTAL

Materials

The sample used in this study was commercial polypropylene (intrinsic viscosity $[\eta] = 3.0$ dl g^{-1}, determined in decalin at 135°C). Relationships between shear stress and shear strain rate were obtained at 200°C with a capillary viscometer fitted with a die of diameter $D = 2$ mm and length to diameter ratio $L/D = 0.5 \sim 10$. End corrections were evaluated from plots of driving pressure *versus* L/D values[7]. The Rabinowitsch equation[8] was applied in this study in order to determine the true rate of shear. In *Figure 1*, shear viscosities for the sample at 200°C are plotted as a function of shear strain rate. The steady state shear viscosity was estimated at 2×10^5 poise. The polymer melt was extruded at 250°–270°C through a die with a single orifice. The screw extruder was fitted with a gear metering pump (Shimadzu Seisakusho Ltd). The die diameters were 2.0 and 1.0 mm and the lengths 45 mm. The extruded rod was taken up without extension. The rods so made had diameters of 2.0, 1.45 or 1.0 mm.

0032–3861/80/020164–07$02.00

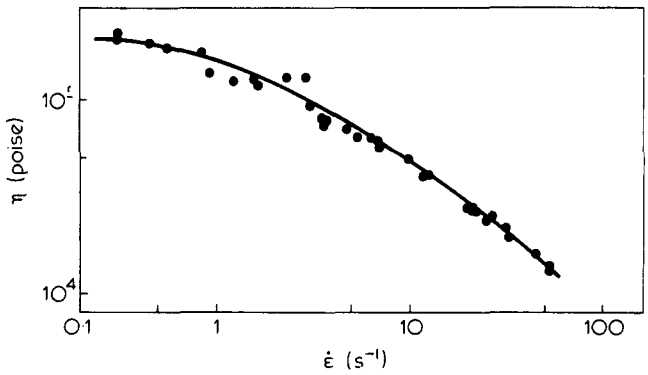

Figure 1 Shear viscosity *versus* shear strain rate for polypropylene melt at 200°C

Apparatus

Figure 2 is a schematic diagram of the apparatus. Its main components are a silicone oil bath (M), a rotating roll clamp (G), tensile testing parts (N, B, D) and a microscope (arrow). The constant-temperature bath was controlled by the arrangement of the pipe heaters and copper plates (similar to Meissner's apparatus). Temperature was measured by thermocouples. The silicone oil used has low density, low viscosity and is transparent. The rotating clamp had a pair of flat gears with a small module. Rotation speed was varied giving values of $\dot{\gamma}$ from 0.002 to 0.6 s^{-1}. The clamp situated in the tensile testing parts used a pair of glass tubes. We tested a rotational clamp consisting of a pair of gears instead of glass tubes. Both clamps gave similar results but the glass tube clamp produced greater precision with small tensions than did a gear clamp. Phosphor bronze plates were used as the leaf spring. The displacement of the leaf spring was measured by a differential transducer. The tensile testing system was calibrated by several small weights, and plots of displacement *versus* weight are rectilinear. For measuring the rod diameter, an incident-light microscope was attached at the position of the arrow. The elongating rod was allowed to settle on an aluminized slide. Light fell incident to the rod by use of a beam-splitting prism. During elongation, the rod was photographed through the microscope and its diameter determined. The scale of the photomicrographs was established by photographing a micro-inscribed scale slide. The rod length between the clamps was 37, 54 or 71 cm. Since the rods exhibited some shrinkage in the bath, 5 min equilibration time was allowed before the beginning of the experiment.

RESULTS

Rod diameter

Elongational strain is defined after Hencky by:

$$\gamma = \int_{t_0}^{t} \frac{dl}{dt} = \ln \frac{l}{l_0} \qquad (1)$$

and corresponding elongational strain rate by:

$$\dot{\gamma} = \frac{1}{l} \frac{dl}{dt} \qquad (2)$$

l_0 and l are the initial and the instantaneous length of the sample. With respect to the apparatus in *Figure 2*, elongational strain rate can be described by the sample length ($L = l$) and take-up speeds of rotational clamps ($V = dl/dt$). Given that sample length and take-up speed are constant, elongational strain rate is constant. With the assumption that the melt under test is incompressible, the rod diameter $d(t)$ is given by the equation:

$$\ln d(t) = \ln d_0 - \frac{\dot{\gamma}}{2} t \qquad (3)$$

where d_0 is the diameter of the sample at time zero.

It should be noted that the initial diameter at the experimental temperature is larger than that at room temperature, because of some volume expansion due to temperature elevation and length shrinkage due to disorientation and surface tension. Initial diameter was measured via the microscope, five min after attainment of the required temperature. Rod diameter *versus* elongational time is shown in *Figure 3* for a series of runs at 200°C, $\dot{\gamma} = 0.05\ s^{-1}$. The homogeneity of elongational deformation was checked by measuring the

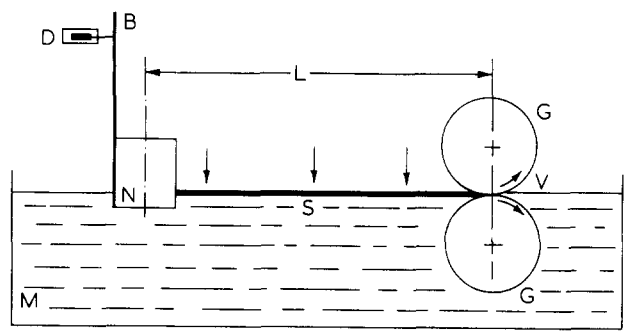

Figure 2 Schematic diagram of elongational rheometer (see text for details)

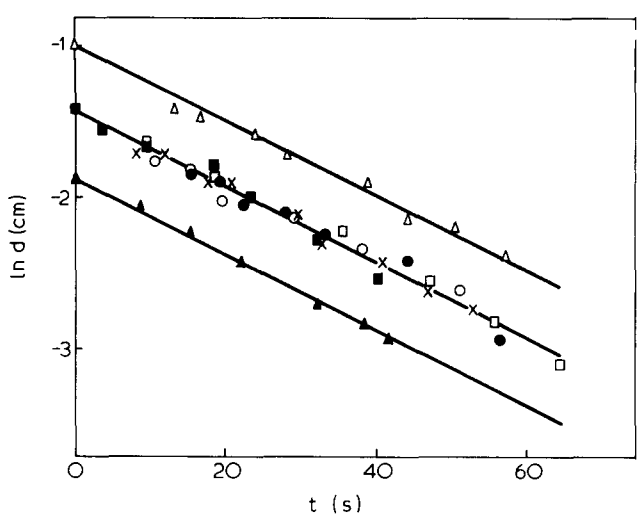

Figure 3 Plots of ln*d versus* time for elongational strain rate 0.05 s^{-1} at 200°C. Solid lines are calculated value from equation (3)

Run no	1	2	3	4	5	6	7
Symbol	x	■	□	●	○	▲	△
d (cm)	0.145	0.145	0.145	0.145	0.145	0.100	0.200
L (cm)	54	54	54	37	71	54	54
X_m (cm)	14	27	41	14	14	14	14

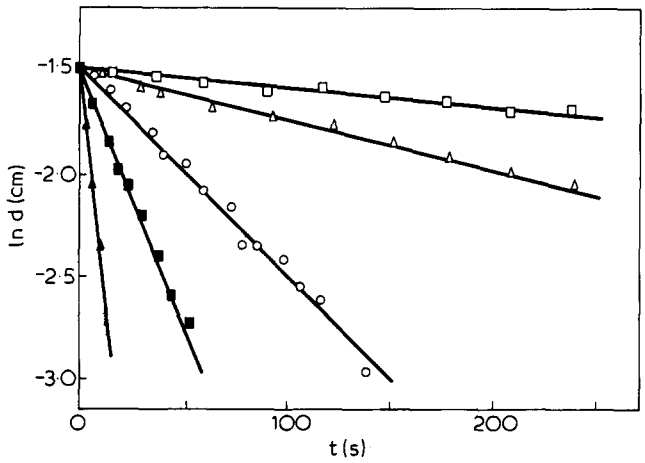

Figure 4 Plots of ln*d versus* time for various elongational strain rates at 200°C. Solid lines are calculated values from equation (3). Elongational strain rate $\dot{\varepsilon}$ (s^{-1}): (▲), 0.2; (■), 0.05; (○), 0.02; (△), 0.005; (□), 0.002

change of diameter with elongational time in three positions (x = 14, 27 and 41 cm). From comparison of runs 1, 2 and 3 in *Figure 3*, diameter inhomogeneity does not seem to affect measured quantities of elongational viscosity within the accuracy of our experiments.

The influence of clamping the molten sample on elongational deformation should be checked. Checks on clamping stability were made by changes in initial sample diameter (d_0 = 0.100, 0.145 and 0.200 cm) and in sample length (L = 37, 54 and 71 cm). The variation of the diameter with time gave similar results for various sample lengths. Therefore, it can be concluded that in this experimental condition the influence of the clamp on elongational experiments is very small. For various initial sample diameters, the same value of slope was found. This means that secure clamping of the melt was obtained.

The natural logarithm of diameter *versus* time is plotted at constant temperature (200°C) during various elongational rates (*Figure 4*). A linear relationship is found for the range of elongational strain rates 0.002–0.2 s^{-1}. In *Figures 3* and *4*, the solid line was calculated from revolutions min^{-1} of the rotating clamp. A comparison of diameter measured by the microscope with calculated diameter is made in these Figures, establishing good fits independent of various experimental conditions.

Cogswell and Moore[9] reported that in simple elongational experiments the linear polymer melt became unstable and necked at a critical elongational strain of 1. They interpreted the result in terms of the Considere constriction which explains necking behaviour in solid polymers. If necking occurs in elongational experiments, at some point the sample diameter would either decrease drastically or not change with time. However, *Figures 3* and *4* show that sample diameter is changed evenly with time. Thus, the polypropylene melt could be elongated without necking, up to high elongational strain of 3–5 in these experiments.

Elongational viscosity

During elongation (*Figure 2*), several forces act on the sample, notably applied take-up force, inertial force, gravity force, frictional drag, and surface tension. The gravity of the sample can be neglected because of buoyancy compensation by the silicone oil. Considering that the surface tension is small, the force balance is:

$$F_x = F_0 - W(V_0 - V_x) - \int_0^x \pi R \rho_p V_x^2 C_f dx \qquad (4)$$

where subscript 0 refers to the rotating clamp position, subscript L refers to the other end, and F_x is $\pi R^2 \sigma$ evaluated at position x. The relationship between take-up force F_0 and measuring force F_m is given by:

$$F_0 = F_m + WV_0 + \int_0^L \pi R \rho_p V_x^2 C_f dx \qquad (5)$$

The density of the polymer melt ρ_p is obtained from dilatometry[10]. For the drag coefficient C_f, equation (6) given by Kase and Matsuo[11] is used:

$$C_f = 1.23 \left(\frac{2RV_x \rho_s}{\mu_s} \right)^{-0.81} \qquad (6)$$

where the density of silicon oil ρ_s ranges from 0.87 g cm^{-3} at 180°C to 0.85 g cm^{-3} at 220°C with respective viscosities of silicon oil μ_s of 0.1 poise at 180°C to 0.08 poise at 220°C. In equation (4), the elongational force depends on x, T, L and V. Thus, the elongational force depends not only on the position but on the diameter and length of sample, the elongational time and elongational strain rate.

Typical distribution of the force components is shown in *Figure 5*. The elongational force was 735 dyn at the rotating clamp position and 721 dyn at the measuring position. The inertia force was about 0.02% of the measured force, and therefore negligible. The frictional force was about 2% of the measured force. However, the fraction of the friction force becomes much larger as elongational strain and elongational strain rate are increased. At γ = 4 with $\dot{\gamma}$ = 0.6 s^{-1}, the frictional force is about 10% of the measuring force. Therefore, the force correction becomes more important as elongational strain or elongational strain rate is increased. An average rheological force over a sample length is corrected for the frictional drag force contribution and defined as the elongational force.

Figure 6 illustrates the dependence of elongational viscosity on elongational strain rate at 200°C for polypropy-

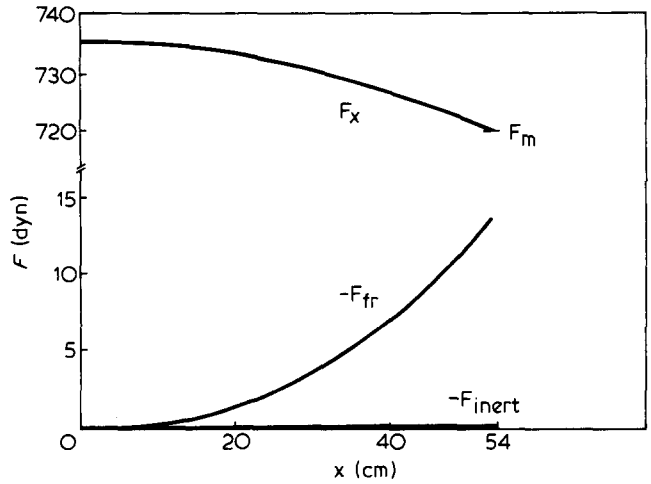

Figure 5 Distribution of the force components at T = 200°C, $\dot{\gamma}$ = 0.05 s^{-1} and t = 10 s

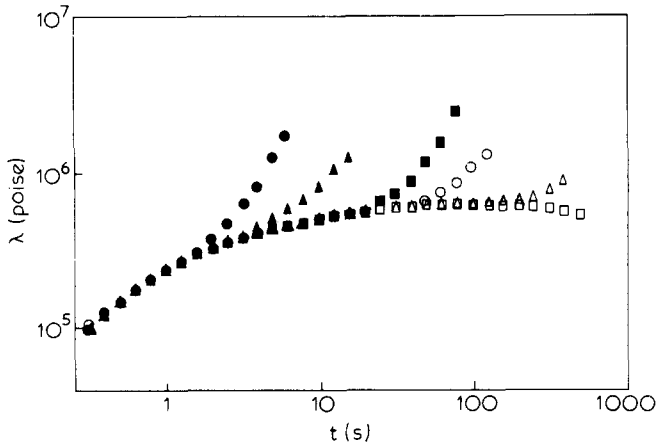

Figure 6 Variation of elongational viscosity with time at a constant elongational strain rate at 200°C. Elongational strain rate (s^{-1}): (●), 0.6; (▲), 0.2; (■), 0.05; (△), 0.02; (○), 0.005; (□), 0.002

lene. When the sample diameter and the sample length between clamps were changed, the same behaviour was obtained. From measurements with different sample diameters and lengths it could be proposed that results of our elongation experiments with constant elongational strain rates are independent of geometry and, therefore, they should be reliable. Although the measured force had some scatter from run to run, elongational stress and/or elongational viscosity varied little, because of compensation due to the initial diameter when the sample melted. *Figure 6* shows that the elongational viscosity increases smoothly with time for the small elongational strain rate ($\dot{\gamma}$ = 0.002 s^{-1}) and reaches the constant value $\lambda = 6 \times 10^5$ poise, equal to $3\eta_0$ in *Figure 1*. For greater values of elongational strain rate, elongational viscosity first increases smoothly with time, until a critical time is reached. This behaviour is similar to that for small elongational strain rates. Beyond the critical time, elongational viscosity increases more rapidly. The critical time decreases with increasing elongational strain rate. In general terms these results are similar to those obtained by Meissner and others[3-6].

Cogswell[12-14] measured elongational viscosity of polymer melts using constant stress elongation. Specimen length was measured by clamp separation and a constant strain rate obtained. These elongational strain rates correspond to the range 0.01 s^{-1}–0.04 s^{-1}. The elongational viscosity of low density polyethylene containing long branches increased with elongational stress; but elongational viscosity of linear polyolefins depended little on elongational stress at low stress levels and decreased slightly with increasing elongational stress. Cogswell's experimental conditions (e.g. $\dot{\gamma}$ = 0.016 s^{-1} and $\dot{\gamma}$ = 0.04 s^{-1}) correspond to the region (t = 5–35 s and t = 5–20 s) of a smooth and small increase in, and the attainment of a constant value of, elongational viscosity (*Figure 6*). Furthermore, our results in this region show that, at constant time, elongational viscosity is almost independent of elongational stress; and, at constant strain, elongational viscosity keeps a constant value or decreases slightly with increasing elongational stress. For example, in the case of γ = 0.5, the elongational viscosity at $\dot{\gamma}$ = 0.005 s^{-1} and $\sigma = 3.2 \times 10^3$ dyn cm^{-2} is 6.3×10^5 poise; and at $\dot{\gamma}$ = 0.05 s^{-1} and $\sigma = 2.4 \times 10^4$ dyn cm^{-2} is 4.8×10^5 poise.

Temperature dependence of elongational viscosity

Elongational viscosity is strongly dependent on temperature. In *Figure 7*, the influence of temperature on elongational viscosity of a polypropylene melt is shown. In the case of small elongational strain rate ($\dot{\gamma}$ = 0.005 s^{-1}), elongational viscosity decreases by about a factor of four as temperature increases from 180° to 220°C. The difference between elongational viscosities at 180°C and 220°C is relatively small after shorter times, and becomes large after longer times. The time taken to reach the steady state is shorter at the high temperature, because increasing temperature will decrease the relaxation time. More significantly, elongational viscosity–time curves evidently have similar shapes at different temperatures. This similarity provides the basis for an important empirical method known as the 'method of reduced variables', which combines data taken at three temperatures into one master curve for the sample. If the activation energy at each time is estimated by an Arrhenius plot, it increases smoothly and reaches a plateau; i.e. it is considered that the activated volume for elongational flow slowly increases and reaches a constant value at about 10 sec. The activation energy in the steady state is 16 kcal mol^{-1}. It should be noted that, with higher elongational strain rates ($\dot{\gamma}$ = 0.05 s^{-1} and $\dot{\gamma}$ = 0.6 s^{-1}), a master curve is also obtained by vertical shift alone. It then becomes evident that the onset of rapid elongational viscosity development from the linear superposed curve is probably independent of temperature. Similar experiments were carried out for samples with various initial diameters and similar temperature dependence was derived. From these results, it appears that the heat of deformation and sample irregularities are almost negligible.

DISCUSSION

For growth of uniaxial elongational stress it has been proposed by Lodge[15] that the stress $\sigma(t)$ may be represented by the equation:

$$\sigma(t) = \int_{-\infty}^{t} \mu(t,t')\,\gamma(t,t')\,dt' \tag{7}$$

where γ is the strain tensor and $\mu(t,t')$ is the memory function of the form:

$$\mu(t-t') = \sum_{k=1}^{N} A_k \exp\left(-\frac{(t-t')}{\tau_k}\right) \tag{8}$$

where A_k and τ_k are constant. The elongational viscosity at the constant elongational strain rate is given by the equation:

$$\lambda(t) = \sum_{k=1}^{N} A_k \left(3 - 2\tau_k \nu_k \exp(-u_k t) - \tau_k u_k \exp(-\nu_k t)\, u_k^{-1} \nu_k^{-1}\right)$$

$$u_k = \tau_k^{-1} - 2\dot{\gamma}, \qquad \nu_k = \tau^{-1} + \gamma \tag{9}$$

Chang and Lodge[16] compared Meissner's data with equation (9). In their calculation, the memory function was assumed arbitrarily to have five terms and a five term version of equation (9) was used consequently to fit the data at the lowest elongational strain rate. Ide and White[6] also noted experimental data of earlier investigators and attempted to fit their own data to a similar equation.

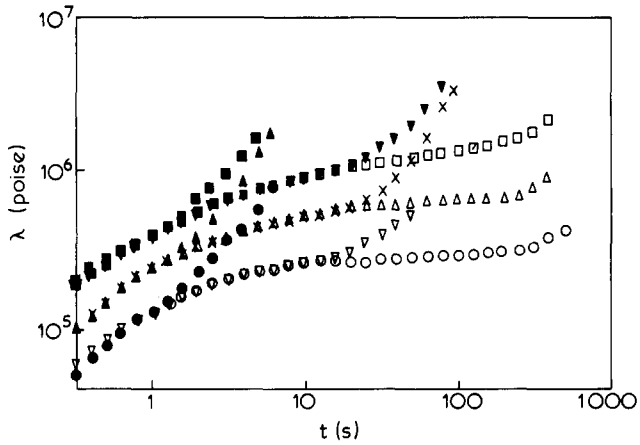

Figure 7 Temperature dependence of the elongational viscosity–time curves at a constant elongational strain rate. Temperature (°C), elongational strain rate (s^{-1}): (●), 220, 0.6; (▽), 220, 0.05; (○), 220, 0.005; (▲), 200, 0.6; (x), 200, 0.05; (△), 200, 0.005; (■), 180, 0.6; (▼), 180, 0.05; (□), 180, 0.005

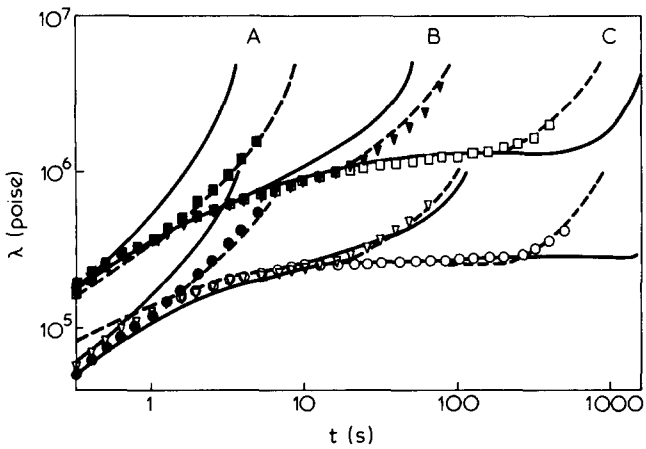

Figure 8 Variation of elongational viscosity with time at a constant elongational strain rate at 220°C and 180°C. The solid lines are deduced from equations (9) and (10) and the broken lines are deduced from equation (16) by use of the parameter fitted to the data at 200°C and 0.002 s^{-1}. Elongational strain rates (s^{-1}): A, 0.6; B, 0.05; C, 0.005

Here, we will deal with the effect of temperature on elongational viscosity. In equation (7), the temperature effect can be included in the time constant τ_k of the memory function. We assume the method of reduced variables for equation (8), like that for linear viscoelastic properties. Then, in equation (8) the time constant τ_k is given by:

$$\tau_k = a_T \tau_k^0 \qquad (10)$$

where a_T is the shift factor and τ_k^0 is the time constant at the reference temperature. The elongational viscosity at various temperatures can be obtained by replacing τ_k with $a_T\tau_k$ in equation (9). *Figure 8* shows the comparison of experimental data with the prediction of equations (9) and (10). The solid lines are theoretical; one is plotted from the results of equation (9). In these calculations, the constant a_k is chosen by matching equation (9) to the data obtained at T_0 = 200°C and $\dot{\gamma}$ = 0.002 s^{-1} which appear to tie in with the linear viscoelastic regime. The constant a_k was 8.27 × 10^5, 8.22 × 10^4, 1.10 × 10^3, 2.33 × 10^{-1} and 3.19 × 10^{-7} when the time constant τ_k was 0.1, 1, 10, 100 and 1000, respectively. Then the shift factor a_T at 180° and 220°C is chosen to fit the data at longer times for $\dot{\gamma}$ = 0.002 s^{-1}. The shift factor a_T is 1.45 at 180° and 0.67 at 220°C; from these values, the activation energy ΔH_L = 7 kcal mol^{-1} is obtained. Theoretical and experimental values compare favourably for linear parts of the elongational viscosity–time curves in this Figure. At high temperature, the theoretical curve is saturated quickly; but at low temperature, it is saturated slowly. This prediction gives a relatively good interpretation of the experimental data. However, for the non-linear parts of the elongational viscosity–time curves, the theoretical curve and experimental data are very different; the theoretical curve is too high at large elongational strain rates and is too low at small elongational strain rates compared with the experimental data. Although the shape of non-linear parts of experimental data is quite similar for different temperatures, that of the theoretical curve changes with temperature. These results suggest that the Lodge model is good for the linear parts but insufficiently explains the non-linear parts. Therefore, it seems reasonable to consider the linear and non-linear parts by different models.

Non-linearity is characterized as follows. *Figure 9* is a typical trace of elongational viscosity during an elongational run. The part from O–A is one of relatively rapid change in elongational viscosity. This is followed by a longer period of slow change from A–B. Up to point B the curve is independent of elongational strain rate at the same temperature: a curve common to all elongational strain rates which has a linear viscoelastic behaviour. The rapid increase of elongational viscosity which is a non-linear effect begins at B, a point approximately independent of temperature. Total elongational strain at B seems independent of elongational strain rate (*Figure 7*). However the accurate assessment of the position of point B in elongational strain is difficult. In order to eliminate this difficulty, many different treatments and plots of experimental data were attempted. We obtain the best plot as follows. The value of elongational viscosity (λ_{exp}) divided by the value of superposed linear viscoelastic data (λ_l) is obtained, which defined the parameter of the non-linearity (λ_n). Plotting of $\ln\lambda_n(t)$ against elongational strain gives two straight lines. In the linear part, $\lambda_n(t)$ is independent of elongational strain and is unity. In non-linear parts, $\ln\lambda_n(t)$ is proportional to elongational strain. The critical elongational strain γ_c is defined by the point of intersection of two straight lines. For experimental results of various elongational strain rates, a straight line

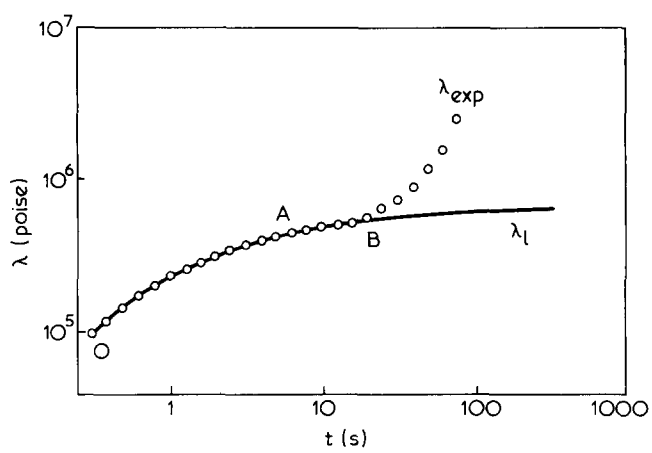

Figure 9 Typical trace of the elongational viscosity–time curve. The parameter of non-linearity (λ_n) is defined by λ_{exp}/λ_l

relationship can be obtained for the data points and the critical point B can be assessed by the critical elongational strain $\gamma_c = 0.7$ which is independent of elongational strain rate. This critical elongational strain was also independent of temperature. Furthermore, the slope of the straight line is 0.16 and almost independent of both elongational strain rate and temperature.

Now, solely considering the linear viscoelastic behaviour, the transient elongational viscosity at the beginning of elongational flow with constant elongational strain rate in a fluid which is initially at rest is given[17] by:

$$\lambda_l(t) = \int_0^t \int_{-\infty}^0 H \exp\left(-\frac{u}{\tau}\right) d\ln\tau du \qquad (11)$$

where H is the relaxation spectrum. Differentiation of the viscosity–time curve yields the relaxation modulus:

$$\frac{d\lambda_l}{dt} = \int_{-\infty}^{\infty} H \exp\left(-\frac{t}{\tau}\right) d\ln\tau = E(t) \qquad (12)$$

Then the temperature reduction of the relaxation modulus can be obtained by plotting $E_T(t)T_0\rho_0/T\rho$ *versus* t/a_T, where $E_T(t)$ is the relaxation modulus at temperature T, T_0 and ρ_0 are the reference temperature and density at T_0, respectively, and a_T is the shift factor. The composite curve shown in *Figure 10* is achieved by empirical shifting of the data at different temperatures through a logarithmic time to $T = 200°C$. The shift factor is 2.0 at 180°C and 0.4 at 220°C. These shift factors give an activation energy of 14 kcal mol^{-1}, which falls between that derived directly from viscosity data and that from the Lodge model. Further, by the Rouse theory[17], one can show that the tensile relaxation modulus is given by:

$$E(t) = A \sum_{p=1}^{N} \exp\left(-\frac{t}{\tau_{max}} p^2\right) \qquad (13)$$

where A is a constant and τ_{max} is the maximum relaxation time. In order to fit the data of tensile relaxation modulus with equation (13), only two parameters of A and τ_{max} can be varied. Then, the curve fitting parameters can be calculated as $A = 8 \times 10^4$ and $\tau_{max} = 5$. The calculated results are shown in *Figure 10*. These parameters and equations (10), (11) and (13) predict the temperature dependence of the linear parts of the viscosity–time curve. Non-linearity of elongational viscosity may be written as:

$$\lambda_m = \frac{\lambda_{exp}}{\lambda_l} = \exp(\alpha\gamma^*) \qquad (14)$$

where α is constant and γ^* is the effective elongational strain and is given by:

$$\gamma^* = \gamma - \gamma_c, \quad \gamma > \gamma_c$$
$$\gamma^* = 0, \quad \gamma \leqslant \gamma_c \qquad (15)$$

The constant α is 0.37 and γ_c is 0.7 for polypropylene. Using equations (10), (11), (12), (13), (14) and (15), the temperature dependence of the elongational viscosity–time curves at a given elongational strain rate becomes:

$$\lambda = \exp(\alpha\gamma^*) A \sum_{p=1}^{N} \frac{a_T \tau_{max}}{p^2} \left\{1 - \exp\left(-\frac{P^2 t}{a_T \tau_{max}}\right)\right\} \qquad (16)$$

The results of the numerical calculation are shown in *Figure 8* by the broken lines. In this figure, a comparison of this calculated curve with the experimental value shows a small discrepancy in the short time region. However, taking into account the difficulties of experimental technqiues during short periods and the simple model used in the calculation, the agreement is fairly good at all elongational strain rates and temperatures.

In addition to these results, non-linearity can be more favourably accorded with experimental data by equation (16) than that by equations (9) and (10) of the Lodge model.

It is interesting to consider the molecular characteristics necessary to produce non-linearity in elongational viscosity. However, in attaining the steady state of shear viscosity at the onset of steady shearing flow, non-linearity was also reported[19,20,21] and referred to as 'stress overshoot'. If a constant shear rate in the range of sufficiently low shear strain rate is imposed, the shear viscosity grows monotonically to its steady state value e.g. the elongational viscosity in the low elongational strain rate. At higher shear strain rates, the shear viscosity, (which is distinct from the elongational viscosity), deviates downward from its steady state value and passes through a maximum before eventually approaching the steady state. The time to reach the maximum t_m is found to be inversely proportional to shear strain rate: $t_m\dot{\epsilon}$ = constant. Therefore, for a given polymer, the total shear strain at the viscosity maximum is constant and independent of $\dot{\epsilon}$ and has a typical value in the range of 2.0–3.0 shear units. Here, stress overshoot can be understood qualitatively in molecular terms by the theory of

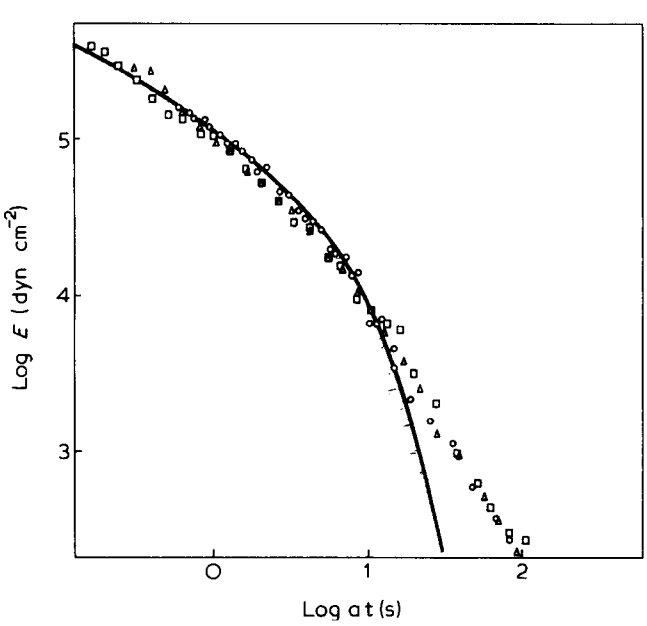

Figure 10 Master curve of relaxation modulus *versus* log($a_T t$): (○), $T = 220°C$; (△), $T = 200°C$; (□), $T = 180°C$. Solid line is calculated from equation (13) using $A = 8 \times 10^4$ and $\tau_{max} = 5$

Graessley[22] in which the reduction of shear viscosity with shear strain rate in non-Newtonian flow is attributed to a reduction in the concentration of entanglement coupling with shear strain rate. In shear viscosity–time experiments, it takes time for the onset of reduction in entanglement to be accomplished. At the beginning, shear viscosity tends towards the Newtonian viscosity value instead of the non-Newtonian value, and it approaches the steady-state value which is non-Newtonian. If these considerations are applied to the elongational viscosity–time experiment, the non-linearity of elongational viscosity is related to the structure change which can be specifically described in terms of entanglement coupling.

Furthermore, the structure change implies an increment in the concentration of the entanglement or in the efficiency of the entanglement coupling, because the elongational viscosity in the non-linear region is larger than that in the steady state region, where the linear viscoelastic behaviour can be shown.

Consequently, polymer melts at rest may contain some concentration of an effective structure, but this is not changed at small elongational strain rates and small elongational strains. However, at large elongational strain rates and large elongational strains the effective structure is destroyed and a new effective structure develops: for large elongational strains, configurational changes of the entangled network are accompanied by a significant decrease in entropy and an increase in molecular orientation along the direction of flow. This gives rise to an increase in elongational stress along the flow line and higher elongational viscosity. The beginning point of such a structural change is defined by the elongational strain, i.e. an overall deformation. In addition, the structural change is accelerated by an overall elongational strain, represented by equation (14).

ACKNOWLEDGEMENTS

The authors are indebted to Mr. H. Moriya and Mr. N. Nishigoori for help with some of the experiments. This work was partially supported by a Grant-in-Aid for Scientific Research from the Japanese Ministry of Education.

REFERENCES

1 Trouton, F. T. *Proc. Roy. Soc.* 1906, **A77**, 426
2 Ballman, R. L. *Rheol. Acta.* 1965, **4**, 137
3 Meissner, J. *Rheol. Acta.* 1969, **8**, 78
4 Meissner, J. *Rheol. Acta.* 1971, **10**, 230
5 Everage, A. E. and Ballman, R. L. *J. Appl. Polym. Sci.* 1976, **20**, 1137
6 Ide, Y. and White, J. L. *J. Appl. Polym. Sci.* 1978, **22**, 1061
7 Bagley, E. B. *J. Appl. Phys.* 1957, **28**, 624
8 Rabinowitsch, B. *Z. Phys. Chem. (A)* 1929, **145**, 1
9 Cogswell, F. N. and Moore, D. R. *Polym. Eng. Sci.* 1974, **14**, 573
10 Danusso, F., Maraglio, G., Ghigla, W., Motte, L. and Talamini, G. *Chim. Ind.*, 1959, **XLI**, 748
11 Kase, S. and Matsuo, T. *J. Polym. Sci.* 1967, **11**, 251
12 Cogswell, F. N. *Plast. Polym.* 1968, **36**, 109
13 Cogswell, F. N. *Polym. Eng. Sci.* 1972, **12**, 64
14 Cogswell, F. N. *Appl. Polym. Symp.* 1975, **27**, 1
15 Lodge, A. S. 'Elastic Liquids', London, 1964, Ch 6
16 Chang, H. and Lodge, A. S. *Rheol. Acta.* 1972, **11**, 127
17 Ferry, J. D. 'Viscoelastic Properties of Polymers', New York, 1970, Ch 3
18 Rouse, P. E. *J. Chem. Phys.* 1953, **21**, 1292
19 Sakai, M., Fukaya, H. and Nagasawa, M. *Trans. Soc. Rheol.* 1972, **16**, 635
20 Takahashi, M., Masuda, T. and Onogi, S. *Proc. 26th Cong. Soc. Rheol. Japan*, 1978, p 89
21 Stratton, R. A. and Butcher, A. F. *J. Polym. Sci. (Polym. Phys. Edn)* 1973, **11**, 1747
22 Graessley, W. W. *J. Chem. Phys.* 1967, **47**, 1942